

RESEARCH

Open Access



Mild hyperthermia via gold nanoparticles and visible light irradiation for enhanced siRNA and ASO delivery in 2D and 3D tumour spheroids

Daniela Ferreira^{1,2}, Alexandra R. Fernandes^{1,2*} and Pedro V. Baptista^{1,2*}

*Correspondence:
ma.fernandes@fct.unl.pt;
pmvb@fct.unl.pt

¹ Associate Laboratory i4HB—Institute for Health and Bioeconomy, NOVA School of Science and Technology, NOVA University Lisbon, 2819-516 Caparica, Portugal
² UCIBIO—Applied Molecular Biosciences Unit, Department of Life Sciences, NOVA School of Science and Technology, NOVA University Lisbon, 2819-516 Caparica, Portugal

Abstract

Background: The delivery of therapeutic nucleic acids, such as small interfering RNA (siRNA) and antisense oligonucleotides (ASO) into cells, is widely used in gene therapy. Gold nanoparticles (AuNPs) have proved to be effective in delivering silencing moieties with high efficacy. Moreover, AuNPs offer the possibility of spatial–temporal triggering of cell uptake through light irradiation due to their unique optical properties. Our study focuses on the use of AuNPs as improved vectorisation agents through mild phototherapy triggered by visible light irradiation. This method promotes the transfection of oligonucleotides for gene silencing in 2D cells and more complex 3D spheroids.

Results: Improving gene silencing strategies in 3D cell cultures is crucial since it provides more effective in vitro models to study cellular responses that closely resemble the in vivo tumour microenvironment. We demonstrate the potential of mild phototherapy by effectively silencing the *GFP* gene in 2D cell cultures: HCT116 and MCF-7. Then we showed that mild phototherapy could be effectively used for silencing the *c-MYC* oncogene transcript, which is greatly overexpressed in cancer cells. A decrease of 25% and 30% in *c-MYC* expression was observed in HCT116 2D cells and 7-day 3D spheroids, respectively.

Conclusions: In summary, our findings offer a novel transfection approach for gene therapy applications in 2D and 3D tumour models. This approach is based on the use of mild phototherapy mediated by AuNPs combined with visible laser irradiation that might pave the way for the spatial–temporal control of gene modulation.

Keywords: Mild hyperthermia, Gold nanoparticles, Gene silencing, Laser irradiation, Therapeutic nucleic acids transfection, 3D tumour spheroids

Background

Efficient delivery of therapeutic nucleic acids, such as small interfering RNA (siRNA) and antisense oligonucleotides (ASO), into cells is a crucial aspect of gene therapy (Ferreira et al. 2020; Khorkova et al. 2023; Mollé et al. 2022; Zhang et al. 2023; Zhu et al. 2022). Ideally, these agents should be vectorised into target cells with maximal



© The Author(s) 2024. **Open Access** This article is licensed under a Creative Commons Attribution 4.0 International License, which permits use, sharing, adaptation, distribution and reproduction in any medium or format, as long as you give appropriate credit to the original author(s) and the source, provide a link to the Creative Commons licence, and indicate if changes were made. The images or other third party material in this article are included in the article's Creative Commons licence, unless indicated otherwise in a credit line to the material. If material is not included in the article's Creative Commons licence and your intended use is not permitted by statutory regulation or exceeds the permitted use, you will need to obtain permission directly from the copyright holder. To view a copy of this licence, visit <http://creativecommons.org/licenses/by/4.0/>. The Creative Commons Public Domain Dedication waiver (<http://creativecommons.org/publicdomain/zero/1.0/>) applies to the data made available in this article, unless otherwise stated in a credit line to the data.

transfection efficiency with minimal toxicity, preferably with spatiotemporal control over the uptake (Carballo-Pedrares et al. 2023; Fus-Kujawa et al. 2021; Wang et al. 2023). Gold nanoparticles (AuNP) are optimal for vectorisation, since they protect oligonucleotides against nucleases and degradation while providing the possibility to track internalisation without significant cytotoxicity (Hosseini et al. 2023; Hu et al. 2020; Sharma et al. 2022). AuNPs are easily functionalised with ASO and siRNA and, due to their optical properties, offer the possibility to use external actuators (e.g., light, radiofrequency) to trigger cell uptake (Deng et al. 2021; Graczyk et al. 2021; Han & Choi 2021; Kanu et al. 2022; Overchuk et al. 2023; Wang et al. 2022).

Due to their unique optical properties, AuNPs have already demonstrated the potential to be used as photothermal agents using incident laser light sources, including visible and near-infrared light (NIR) (Amendoeira et al. 2020; Hu et al. 2020; Oliveira et al. 2023; Riley & Day 2017). The electromagnetic energy transformed into heat as a result of electron excitation and relaxation by AuNPs is one of their unique physicochemical properties (Xiaohua Huang and El-Sayed 2010; Krajczewski et al. 2017; Kumar et al. 2023). For instance, Braun et al. reported that hollow gold nanoshells conjugated with siRNA and Tat peptides for cellular uptake were trapped within endosomes, which could escape upon exposure to a pulsed NIR laser, allowing the release of siRNA into the cytosol (Braun et al. 2009). Our group has demonstrated the photothermal potential of spherical AuNPs upon visible laser irradiation at the surface plasmon (SPR) peak (Mendes et al. 2017; Pedrosa et al. 2017, 2018; Roma-Rodrigues et al. 2020).

Localised mild hyperthermia shows the possibility of modulating the cell membrane behaviour (e.g., fluidity) and increasing the susceptibility of cells to improve the internalisation of AuNPs functionalised with oligonucleotides for gene therapy. The efficacy of combining spheric functionalised AuNPs with visible laser irradiation to enhance therapeutic outcomes in vitro and in vivo models has been reported (Heinemann et al. 2013; Pedrosa et al. 2017; Roma-Rodrigues et al. 2020).

3D models recapitulate the in vivo tumour microenvironment (TME) to closely resemble tumour growth and progression, which are necessary to better evaluate therapeutic responses (Pinto et al. 2020; Valente et al. 2023). The formation of cell-to-cell and cell-matrix interactions in three-dimensional (3D) cell cultures (e.g., multicellular tumour spheroids and organoids) is a pivotal link between 2D cultures and animal models (Jensen and Teng 2020; Zanoni et al. 2020). Spheroids are excellent in vitro 3D models that can mimic the structure of tumours owing to the formation of a gradient of nutrients, oxygen, pH, and metabolism products, and can also recreate some of their mechanisms, such as hypoxia and acidosis.

Herein, we use light irradiation of AuNPs for the controlled increased delivery of oligonucleotides into 2D cell cultures and 3D tumour spheroids for targeted gene silencing—see Fig. 1.

Materials and methods

AuNP synthesis and functionalisation

AuNPs were synthesised resorting to the citrate reduction method described by Lee and Meisel (Lee and Meisel 1982), and subsequently functionalised with polyethylene glycol (PEG) for improved stability in biological media as previously reported (Baptista

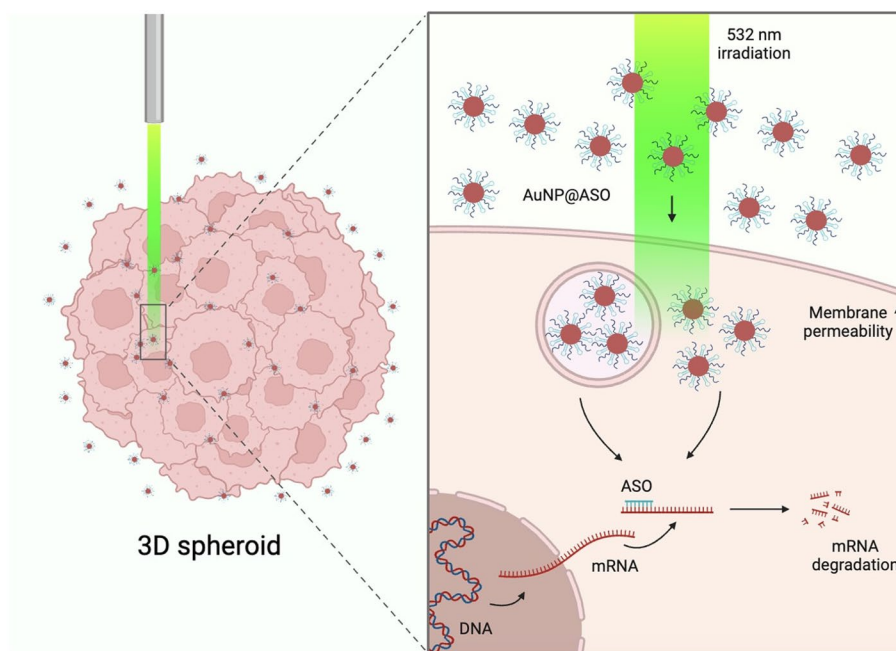


Fig. 1 Overview of the general concept for intracellular delivery of silencing nucleic acids in 3D spheroid. The localised irradiation promotes NP uptake and effective delivery of ASO for gene silencing—triggered by mild hyperthermia (Created with BioRender.com)

et al. 2013)—100% PEG ensures stability in complex media; the 30% coverage allows for “space” for functionalisation with the oligonucleotide, which compensates for the lower % of PEG at the surface in terms of stability. Briefly, to achieve 100% coverage of the AuNPs’ surface, 10 nM of citrate-capped AuNP were incubated with 0.028% SDS (*w/v*) (Sigma-Aldrich, Switzerland) and 0.01 mg/mL of thiolated PEG (M_w :356 Da, Sigma-Aldrich, Switzerland) for 16 h under agitation at room temperature. The excess PEG was removed by centrifugation at 14,000 *g* for 30 min at 4 °C (three times), and the free thiol-PEG was quantified in the supernatants via the Ellman’s Assay. A 100% coverage was considered when the supernatant showed no traces of free thiol, which indicated that all thiol-PEG had been bonded to the AuNP surface.

In addition, AuNPs with a 30% coverage of PEG (AuNP@PEG 30%) were prepared and subsequently functionalised with a thiolated stem-looped ASO complementary to the *c-MYC* transcript (GenBank NM_002467.5; AuNP@*c-MYC*) and a *scramble* oligo (AuNP@*scramble*) as a control, as previously described by Baptista et al. ASO was added at a 1:150 AuNP: oligonucleotide proportion, incubated for 16 h, and the excess oligonucleotides were removed by centrifugation at 15,500 *g* for 1 h at 4 °C and washed twice with diethylpyrocarbonate (DEPC)-treated water (Sigma-Aldrich, Switzerland). The number of ASO functionalised to the surface was inferred from the quantification of single-stranded DNA in the supernatants using a Nanodrop spectrophotometer (ND-1000, NanoDrop Technologies, USA), considering the amount of initially added ASO.

AuNP and Au-nanoconjugates were assessed by ultraviolet–visible absorption spectroscopy (UV–Vis), dynamic light scattering (DLS), zeta potential, and transmission electron microscopy (TEM). UV–Vis spectra were acquired on a UV–Vis spectrophotometer (UV mini-1240 spectrophotometer, Shimadzu, Germany) in the range

400–800 nm using a 1 cm path quartz cuvette (Quartz SUPRASIL, Hellma Analytics, Germany) at room temperature (RT). The hydrodynamic diameter, polydispersity index, and zeta potential were measured by DLS resorting to a Malvern Zetasizer Nano ZS at 25 °C, scattering angle 173° and laser wavelength 633 nm (Malvern, Zetasizer Nano series, United Kingdom). TEM analysis was provided as a service by Instituto Gulbenkian de Ciência (IGC) and the core diameters were calculated using the open-access software platform FIJI—Image J (National Institutes of Health, Bethesda, United States).

Characterisation of AuNP and Au-nanoconjugates can be found in Additional file 1: Table S1, Figures S1 and S2.

Irradiation and photothermal characterisation

To determine the photothermal capability of the Au-nanoconjugates, these were irradiated at different concentrations (0.25 nM, 0.5 nM, 0.75 nM, and 1 nM) in water in a 96 well-plate. For temperature measurements, a thermocouple was inserted in the wells before and immediately after visible light laser irradiation, as previously described (Mendes et al. 2017; Pedrosa et al. 2018). Irradiation was performed with a continuous wave (CW) 532 nm green diode-pumped solid-state laser (DPSS) (Changchun New Industries Optoelectronics Tech. Co., LTD, Changchun, China) with a diode intensity (LDI) of 2.37 W/cm² coupled (Mendes et al. 2017) to an optical fibre for different exposure times (30 s, 60 s, 90 s, and 120 s).

Cell culture maintenance

HCT116 colorectal carcinoma (ATCC[®] CCL-247[™]) was purchased from the American Type Culture Collection (ATCC, Manassas, VA, USA) and MCF-7/GFP breast adenocarcinoma expressing constitutively an optimised version of GFP—copGFP (Cat# AKR-211) was purchased from Cell Biolabs (Cell Biolabs Inc, San Diego, CA, USA). 2D cells were maintained at 37 °C in a 5% CO₂ atmosphere and 99% relative humidity in Dulbecco's modified Eagle's medium (DMEM) supplemented with 10% (v/v) foetal bovine serum (FBS), penicillin/streptomycin (100 U/mL), all purchased from Gibco, USA. MCF-7/GFP was also supplemented with 1% of MEM nonessential amino acid (Gibco, USA).

Upon attaining confluency, 2D cells were trypsinised with TrypLE[™] Express (Gibco, USA), stained with 0.4% Trypan Blue solution (Gibco, USA), counted using a Neubauer chamber (Hirschmann, Germany), and cultured into fresh medium.

For 3D colorectal tumour spheroids, HCT116 cells were seeded at a density of 5×10^3 cells per well in an ultra-low attachment plate (Nunclon[™] Sphera[™] 96-Well, Nunclon Sphera-Treated, U-Shaped-Bottom Microplate, ThermoFisher Scientific, USA). HCT116 3D spheroids were grown for 3 and 7 days in DMEM at 37 °C in a 99% humidified atmosphere and 5% (v/v) CO₂, monitored with Ti-U Eclipse inverted microscope (Nikon, Tokyo, Japan) (Roma-Rodrigues et al. 2020; Valente et al. 2023).

Plasmid transfection with lipofectamine LTX and plus reagent

HCT116 2D cells were placed at a density of 2×10^4 cells/well in a 96-well plate and cultured in DMEM for 24 h at 37 °C, under standard cell culture conditions, prior to transfection. A plasmid that encodes a GFP (λ_{ex} 475 nm/ λ_{em} 505 nm) optimised for high

expression in mammalian cells (pAcGFP1-Nuc Vector 4.8 kb, Takara Bio Company, USA), was added (100 ng/well) to cells using a 1:2 (plasmid: Lipofectamine) ratio and incubated in DMEM (0% FBS and without antibiotics) for approximately 4 h at 37 °C, according to the Lipofectamine LTX and Plus Reagent (Invitrogen, ThermoFisher Scientific, USA) manufacturer's recommendation. AcGFP1 expression was confirmed after 24 h by fluorescence microscopy (Ti-U Eclipse inverted microscope; FITC filter (excitation at 480/30 nm and emission at 535/40 nm)) and images were analysed using Image J software.

Challenge of cells with Au-nanoconjugates

Quantification of AuNP internalisation into cells

The internalisation of the AuNP@PEG 100% in irradiated and non-irradiated HCT116 2D cells was analysed via inductively coupled plasma atomic emission spectroscopy (ICP-AES). For this experiment, HCT116 2D cells were washed with phosphate-buffered saline (PBS), trypsinised with TrypLE™ Express, and centrifuged at 750 *g* for 5 min. The supernatant was removed and stored at 4 °C, whereas the cell pellet was stored at -20 °C. One day before analysis, 1 mL of freshly prepared aqua regia (HCl: HNO₃ = 3:1) was added to the samples. A standard curve for gold was recorded to quantify the amount of intracellular gold (LAQV/REQUIMTE, Laboratório de Análises).

Laser irradiation in 2D cells: HCT116 and MCF-7/GFP

HCT116 and MCF-7/GFP 2D cells were seeded at a density of 2×10^4 /well and 1×10^4 /well respectively, in a 96-well plate and incubated for 24 h at 37 °C in a 99% humidified atmosphere and 5% (*v/v*) CO₂. After 24 h, HCT116 2D cells were transfected with 100 ng of pAcGFP1 Nuc Vector using Lipofectamine LTX and Plus Reagent. After 4 h of incubation with Lipo + pGFP complexes, the culture medium was replaced with DMEM without phenol red, and cells were challenged (or not) with 10 nM of AuNP@PEG 100% for 4 h. Next, the cell culture medium was replaced with DMEM without phenol red (at 37 °C) containing 20 nM of *anti-AcGFP1*. For MCF-7/GFP: following 24 h, cells were challenged (or not) with 10 nM of AuNP@PEG 100% for 4 h, and then cell culture medium was replaced with DMEM without phenol red (at 37 °C) containing 20 nM of *anti-copGFP*.

Cells with AuNP were then irradiated with a continuous wave 532 nm green DPSS laser coupled to an optical fibre (LDI 2.37 W/cm²) for 60 s to achieve mild hyperthermia. Controls without irradiation, with or without AuNP, were also prepared. For temperature measurements, a thermocouple was inserted in the wells (in contact with the cell culture medium) before and immediately after visible light irradiation.

After 6 h and 24 h for copGFP and 24 h for AcGFP1, GFP expression was confirmed by fluorescence microscopy and MTS assay was performed. In addition, total RNA was extracted from irradiated and non-irradiated cells, and the effect of visible irradiation on the transfection of *anti-AcGFP1* and *anti-copGFP* silencing was evaluated by real-time quantitative PCR (RT-qPCR) and compared to a commercial transfection reagent, Lipofectamine RNAiMAX reagent (Invitrogen, ThermoFisher Scientific, USA), using the manufacturer's instructions.

Cells transfection with lipofectamine RNAiMax reagent

HCT116 and MCF7/GFP 2D cells were seeded at a density of 2×10^4 /well and 1×10^4 /well respectively, in a 96-well plate and incubated for 24 h at 37 °C under standard cell culture conditions. After 24 h, 20 nM of oligonucleotide was mixed with the cationic lipid reagent Lipofectamine RNAiMax in DMEM without phenol red (0% FBS and without antibiotics) and incubated for 5 min in a microcentrifuge tube according to the manufacturer's recommendation. Next, this mixture was added to cells in DMEM without phenol red (Final 8% FBS) for 24 h in HCT116 2D cells; and 6 h and 24 h in MCF-7/GFP 2D cells.

Post-transfection incubation, total RNA was extracted, and the efficiency of transfection for *AcGFP1* and *copGFP* silencing was evaluated by RT-qPCR, and fluorescence microscopy for copGFP protein expression.

c-MYC silencing in HCT116 2D cells

HCT116 2D cells were plated at a density of 2×10^4 cells/well in a 96-well plate and incubated for 24 h at 37 °C in a 99% humidified atmosphere and 5% (v/v) CO₂. After 24 h, the cells were challenged with AuNP@ASO and AuNP@PEG in DMEM without phenol red to evaluate *c-MYC* expression at different time points: 6 h, 9 h, 12 h, and 24 h. The concentration of ASO was 50 nM (0.39 nM of AuNP@*c-MYC* and 0.45 nM of AuNP@*scramble*), using 0.39 nM and 0.45 nM of AuNP@PEG 30% as controls, respectively. The cells were then irradiated after 4 h of AuNP incubation with the set laser conditions mentioned above. Total RNA was extracted, and an MTS assay was performed. The effect of visible irradiation in the internalisation of AuNP@ASO for *c-MYC* silencing was evaluated via RT-qPCR and Immunofluorescence assay. Following the initial assessment, the 9 h incubation period was selected for further experiments.

c-MYC silencing in HCT116 3D spheroids

HCT116 2D cells were seeded with a density of 5×10^3 /well in an ultra-low attachment 96-well plate to produce 3D spheroids and incubated for 3 and 7 days at 37 °C, under standard culture conditions. The 3- and 7-day 3D spheroids were challenged with 25 nM and 60 nM of ASO, respectively (0.19 nM and 0.47 nM of AuNP@*c-MYC*; as controls, 0.23 nM and 0.54 nM of AuNP@*scramble*, respectively) in DMEM without phenol red. AuNP@PEG 30% was used for control of AuNP@*c-MYC* (0.19 nM and 0.47 nM) and AuNP@*scramble* (0.23 nM and 0.54 nM). Upon 4 h, HCT116 3D spheroids were irradiated as described above for HCT116 2D cells. Following 9 h of incubation, total RNA was extracted, and LDH assay and LIVE/DEAD Viability/Cytotoxicity assays were performed. The effect of visible irradiation in the internalisation of AuNP@*c-MYC* in silencing was evaluated with RT-qPCR and Immunofluorescence assay.

c-MYC immunofluorescence in HCT116 2D cells/3D spheroids

HCT116 2D cells were fixed with 4% formaldehyde for 20 min, then washed three times with PBS and permeabilised with 0.1% Triton-X 100 in PBS for 5 min. HCT116 3D spheroids were fixed with 4% formaldehyde for 1 h, then washed three times with PBS and subsequently permeabilised using 0.1% Triton-X 100 in PBS for 30 min. Cells were incubated with 7.5 µg/mL of Hoechst 33,258 for 15 min and the spheroids were incubated

for 45 min, then washed three times with PBS and the blocking was performed with 1% bovine serum albumin (BSA) in PBS with 0.1% Tween 20 (PBST) for 1 h. Next, cells and spheroids were incubated overnight at 4 °C with the primary antibody—anti-rabbit *c-MYC* antibody (1:200 dilution; ab32072; Abcam, UK). After incubation, cells and spheroids were washed three times with PBST, and cells were incubated for 1 h at RT with the secondary antibody—FITC-conjugated anti-rabbit antibody (1:500 dilution; ab6717; Abcam, UK), whereas the spheroids were incubated for 3 h. The cells and spheroids were subsequently washed three times with PBST and visualised in PBST using a Ti-U Eclipse inverted microscope. Images were acquired using the DAPI emission filter (excitation at 360/40 nm and emission at 460/50 nm) and FITC emission filter (excitation at 480/30 nm and emission at 535/40 nm). Fluorescence microscopy images were analysed using Image J software.

Membrane integrity and cell viability assays

HCT116 2D cells membrane integrity was evaluated by Trypan Blue exclusion assay. Briefly, irradiated, and non-irradiated cells, previously incubated or not with 10 nM of functionalised AuNP for 4 h were immediately incubated with Trypan Blue dye for 10 min and washed three times with PBS to remove the excess of the dye. For the analysis of membrane integrity of irradiated and non-irradiated cells, with or without AuNP, several images were acquired with a bright field inverted microscope (Nikon TMS, Tokyo, Japan).

The membrane integrity of HCT116 2D cells/3D spheroids (irradiated or not, in the presence or absence of Au-nanoconjugates) was also evaluated by resorting to the release of intracellular lactate dehydrogenase (LDH) in cells supernatant by LDH assay (CytoTox 96 Non-Radioactive Cytotoxicity Assay, Promega, UK). As a positive control for membrane rupture, the application of LDH lysis solution diluted in DMEM (1:10) was prepared 1 h before the procedure and incubated in cells or spheroids. Following the HCT116 2D cells irradiation or 9 h of 3D spheroids challenge with Au-nanoconjugates, 50 µL of cells or spheroids supernatant are incubated with 50 µL of CytoTox 96 Reagent (1:1 ratio) in a 96-well plate for 30 min at RT, protected from light. Next, 50 µL of Stop Solution is added to the wells and incubated for 1 h at RT, in the dark. The absorbance was measured at 490 nm, on a microplate reader Infinite M200 (Tecan, Switzerland) and cell cytotoxicity was normalised to positive control.

2D cell viability (irradiated and non-irradiated cells, with or without AuNP) was evaluated via the MTS assay. Briefly, cells were incubated with the MTS solution (1:5 v/v in DMEM; CellTiter 96 AQueous One Solution Cell Proliferation Assay Kit, Promega, UK) for 1 h, at 37 °C under standard cell culture conditions and the absorbance was measured at 490 nm using a microplate reader. Cell viability was normalised to control cells (cells with culture medium) (Lenis-Rojas et al. 2017; Silva et al. 2013).

LIVE/DEAD Viability/Cytotoxicity assay (Invitrogen, ThermoFisher Scientific, USA) was performed to assess the impact of visible irradiation after the *c-MYC* silencing experiment in HCT116 3D spheroids. Following the 9 h of silencing, the irradiated and non-irradiated spheroids were washed with PBS and incubated with 1 µM of Calcein AM and 2 µM of Ethidium homodimer-1 (EthD-1) in PBS for approximately 45 min, at 37 °C in a 99% humidified atmosphere and 5% (v/v) CO₂. Fluorescence microscopy

images were acquired by a Ti-U Eclipse inverted microscope using an FITC emission filter (excitation at 480/30 nm and emission at 535/40 nm) and G2A emission filter (excitation at 535/50 nm and emission > 590 nm). Fluorescence microscopy images were analysed using Image J software, and the ratio between Calcein AM and EthD-1 was performed to evaluate cell viability/cytotoxicity.

Total RNA extraction, cDNA synthesis, and RT-qPCR assessment of gene silencing

Total RNA was extracted from 2D cultures using the Nzyol reagent (NZYTech, Portugal) according to the manufacturer's guidelines. RNA extracted from HCT116 2D cells transiently expressing *AcGFP1* or MCF-7 constitutively expressing *copGFP* was reverse transcribed to cDNA using the NZY M-MuLV First-Strand cDNA Synthesis kit (NZYTech, Portugal). RT-qPCR was performed using NZYSupreme qPCR Green Master Mix (2x) (NZYTech, Portugal) according to the manufacturer's protocol in a Qiagen Rotor-Gene Q cycler (Qiagen, Germany). The following conditions were used for *AcGFP1*: initial denaturation at 95 °C for 5 min; 30 cycles of 95 °C 30 s, T_m 52 °C for 30 s, 72 °C for 45 s; and a final extension step at 72 °C for 7 min; for *copGFP*: initial denaturation at 95 °C for 5 min; 30 cycles of 95 °C for 30 s, T_m 53 °C for 30 s, 72 °C for 30 s; and a final extension step at 72 °C for 5 min.

Total RNA was also extracted from HCT116 2D cells and six 3D spheroids after *c-MYC* silencing and RT-qPCR was performed using a one-step NZY RT-qPCR Green kit (NZYTech, Portugal) in a Qiagen Rotor-Gene Q cycler. The set conditions for reverse transcription were 50 °C for 20 min, and qPCR with initial denaturation at 95 °C; 30 cycles of 95 °C 15 s, T_m, and extension of 60 °C for 15 s.

Gene expression was evaluated according to the $2^{-\Delta\Delta C_t}$ method (Livak & Schmittgen 2001), using the *18S* ribosomal gene as reference. All primers and antisense oligonucleotides were purchased from STAB VIDA, Lda (Portugal); all sequences can be found in Additional file 1: Tables S2 and S3.

Statistical analysis

Data were analysed using GraphPad Prism 8.0 (GraphPad Software, San Diego, USA). One-way and two-way ANOVA with Tukey's multiple comparison test, and unpaired parametric *t* test with Welch's correction were used to evaluate differences between groups. They were considered statistically significant at *p* value < 0.05. Data are the mean value of at least three independent assays with at least two technical replicates, and the errors are calculated by the standard error mean.

Results and discussion

Synthesis and characterisation of Au-nanoconjugates

Citrate-capped AuNP characterisation by UV-Vis, DLS, and TEM shows a maximum Localised Surface Plasmon Resonance (LSPR) peak at 519 nm, a hydrodynamic diameter of 16.4 (±0.1) nm by DLS, and an average spherical shape of 12.1 (±1.5) nm by TEM. The AuNP@PEG showed a slight red shift of the LSPR peak (520 nm) and a slight increase in the hydrodynamic diameter 21.1 (±0.3) and 18.5 (±0.1) nm for 30% and 100% PEG coverage, respectively. Functionalisation with the ASO resulted in an additional slight right shift of the LSPR peak to 522 nm and average hydrodynamic diameters

for AuNP@*c-MYC* and AuNP@*scramble* were 35.7 (± 0.2) and 35 (± 0.2) nm, respectively (see Additional file 1: Table S1 and Figures S1, S2).

Laser irradiation

The photothermal effect of the Au-nanoconjugates was assessed by irradiating a range of concentrations of pegylated AuNP: 0.25 nM, 0.5 nM, 0.75 nM, and 1 nM; at different exposure times: 30 s, 60 s, 90 s and 120 s. The temperature variation (ΔT) was calculated by subtracting the final temperature from the initial temperature in each assay, excluding the temperature of the irradiated water. The thermal capacity of water 4.18 J.g⁻¹.K⁻¹ (q) and the irradiated mass (m) of 0.1 g were used to estimate the heat via Eq. 1 (Huang et al. 2012; Kim et al. 2023)—Fig. 2a, b:

$$Q = q \times \Delta T \times m \tag{1}$$

For mild hyperthermia a target temperature of 41–42 °C is desirable (Mendes et al. 2017), corresponding to the ΔT values of 4–5 °C attained for both types of pegylated AuNP upon 60 s laser irradiation. Under these conditions, the photothermy effect was determined to be 7.8 $\times 10^{-13}$ W per particle for AuNP@PEG 30% (Fig. 2c and 9.5 $\times 10^{-13}$ W per particle for AuNP@PEG 100% (Fig. 2d). Altogether, these settings were considered to achieve a mild hyperthermia effect in cells.

Cytotoxic and viability assays in HCT116 2D cells

To assess the effect of the selected conditions for mild hyperthermia in cells, HCT116 colorectal carcinoma 2D cells were incubated for 4 h with 10 nM of AuNP@PEG 30% and 10 nM AuNP@PEG 100%, with or without irradiation. The irradiated and

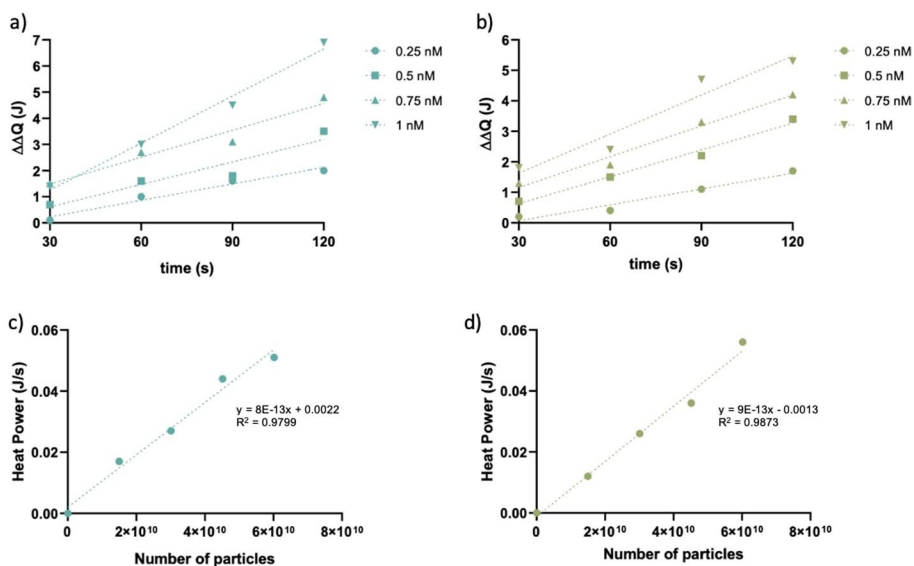


Fig. 2 Heat capacity and heat generated per second of Au-nanoconjugates. Heat capacity of (a) AuNP@PEG 30% and (b) AuNP@PEG 100% for different exposure times and concentrations of AuNP in water irradiated at 2.37 W/cm². Four different concentrations of (c) AuNP@PEG 30% and (d) AuNP@PEG 100% were irradiated at 2.37 W/cm² for 60 s in water and the temperature variation was measured to calculate heat generated per second as a function of the number of particles irradiated. The slope of the curve gives the heat generated per nanoparticle per second

non-irradiated 2D cells were then incubated with Trypan Blue 0.4% (*m/v*) solution and the images acquired in a bright field inverted microscope. Trypan blue is a dye impermeable to live cells which can penetrate necrotic cells or cells with permeable compromised membranes (Strober 2015). Our data show for the used conditions that HCT116 2D cells did not stain with trypan blue (see Additional file 1: Figure S3), despite the slight increase of temperature, showing that the integrity of cell membrane was not compromised by the selected LDI condition: 2.37 W/cm² for 60 s.

HCT116 2D cell viability was further assessed by the MTS assay following the 4 h of incubation with 10 nM of AuNP@PEG 30% and 10 nM AuNP@PEG 100%, with or without irradiation. The MTS assay specifically relies on the activity of mitochondrial enzymes, such as dehydrogenases, which are indicative of the functional and metabolically active cells (Cory et al. 1991; Stoddart 2011). Again, the MTS data indicate that pegylated AuNPs, with or without laser irradiation, do not have an impact on cell viability (Additional file 1: Figure S4a).

To complete the cell viability assessment, we used the LDH assay to simultaneously evaluate cells' membrane permeability and integrity. This assay measures cytotoxicity by quantifying the LDH release in the cell medium and could indicate permeability and/or cell membrane damage (Decker & Lohmann-Matthes 1988; Stoddart 2011). Results show that AuNP@PEG 100% combined with laser irradiation increases 2D cells' membrane permeability, but without compromising membrane integrity as corroborated by the trypan blue exclusion assay (Additional file 1: Figure S4b).

Laser irradiation-induced Au-nanoconjugates uptake

TEM and ICP–AES were used to assess Au-nanoconjugates uptake by cells upon laser irradiation—Fig. 3. TEM images of HCT116 2D cells incubated for 4 h with AuNP@PEG 100% show internalisation of AuNPs in small clusters (Fig. 3a). This clustering is commonly observed for internalisation of the AuNPs (Carnovale et al. 2019; Janic et al. 2018).

Then, we determined the amount of gold inside the cells by ICP–AES in cells that were exposed to 10 nM of AuNP@PEG 100% for 4 h either irradiated or non-irradiated.

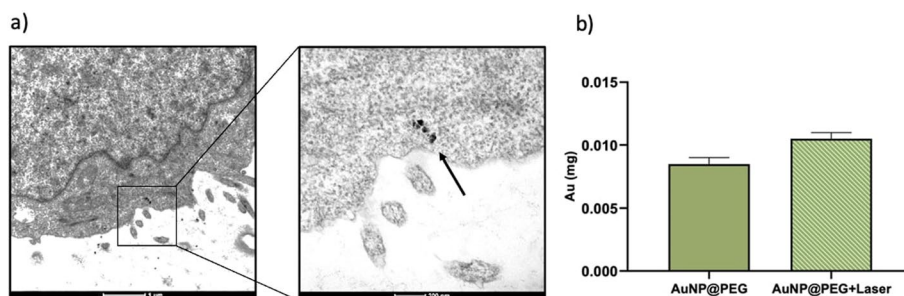


Fig. 3 TEM images of Au-nanoconjugate internalisation in HCT116 2D cells and Au uptake. **a** Images of AuNP@PEG 100% clusters (indicated with a black arrow) inside HCT116 2D cells, observing more than four small dark clusters near to cell membrane due to the high electronic density of gold. Scale bars correspond to 1 μ m and 200 nm, respectively. **b** ICP–AES analysis shows an increase of Au uptake in irradiated cells exposed to 10 nM of AuNP@PEG 100% for 4 h. Statistical differences were not observed between AuNP@PEG and AuNP@PEG + Laser samples. Data represent the mean value \pm the standard error mean of an independent experiment with three technical replicates for each

Data show that irradiated cells (AuNP@PEG + Laser) internalised approximately 1.4-fold more Au when compared to non-irradiated cells (AuNP@PEG)—see Fig. 3b. We hypothesise that the localised heat produced by irradiated AuNP@PEG somehow destabilises the lipid bilayer, increasing fluidity and permeability, which allows an increase in the uptake of pegylated-AuNP by cells. The creation of hotspots on the cell membrane has been observed since that influences the permeability of the membrane (Beola et al. 2020; Kang et al. 2019; Madrid 2018).

Mild phototherapy for GFP silencing in HCT116 2D cells

To demonstrate that mild phototherapy may be used to improve the internalisation of silencing oligonucleotides (antisense siRNA or ASOs) in HCT116 2D cells, AuNP@PEG and an *anti-GFP* were used (Fig. 4a). First, a transient transfection model of HCT116 2D cells harbouring a pAcGFP1–Nuc plasmid that encodes for GFP from *Aequoera coerulescens* with three copies of the nuclear localisation signal (see Additional file 1: Figure S5) was used. After 4 h of plasmid–lipofectamine incubation, the cell culture medium was replaced by DMEM without phenol red, with or without 10 nM of AuNP@PEG for another 4 h at 37 °C.

Then, the cell medium was replaced with DMEM without phenol red at (37 °C), and 20 nM of *anti-AcGFP1* was added before laser irradiation at 2.37 W/cm², for 60 s. The silencing efficiency between the commercially available Lipofectamine RNAiMax and the mild phototherapy mediated by the Au-nanoconjugates was compared for irradiated and non-irradiated cells by assessing *AcGFP1* expression via RT-qPCR and fluorescence microscopy. A control with non-irradiated cells incubated with AuNP@PEG with the *anti-AcGFP1* was used to verify if the presence of AuNP@PEG could promote the intracellular delivery of the silencing oligonucleotide—Fig. 4.

HCT116 cells transiently expressing AcGFP1 protein were observed in a fluorescence microscope after 24 h (Fig. 4b). RT-qPCR data confirmed the silencing of *AcGFP1* for all conditions tested (Fig. 4c). Indeed, irradiated cells with prior incubation with AuNP@PEG (AuNP@PEG + Laser + ASO), showed 70% lower *AcGFP1* expression compared to Control (cells without ASO, $2^{\Delta\Delta Ct} = 1$). This silencing effect was slightly more pronounced than that obtained for the LipofectamineRNAiMax reagent (approximately 65%). In addition, non-irradiated cells with prior incubation of AuNP@PEG (AuNP@PEG + ASO) also showed a significant decrease (approximately 45%) of *AcGFP1* expression compared to control. Irradiation might be causing the increased uptake of AuNPs, which in turn allows for a “dragging” effect of the oligonucleotide into the cell (Elsner 2012; Stewart et al. 2018). Still, laser irradiation has proven a critical trigger for the uptake of the silencing oligonucleotide since laser irradiation with AuNP@PEG (AuNP@PEG + Laser + ASO) reduces the expression of *AcGFP1* 1.8-fold more than without laser irradiation.

None of these conditions showed any impact on cell viability as analysed by the MTS assay (Fig. 4d).

Mild phototherapy for copGFP silencing in MCF-7/GFP cells

We then confirmed the robustness of our approach in the MCF-7 breast adenocarcinoma cell line, which has been reported to be more difficult to transfect with siRNA

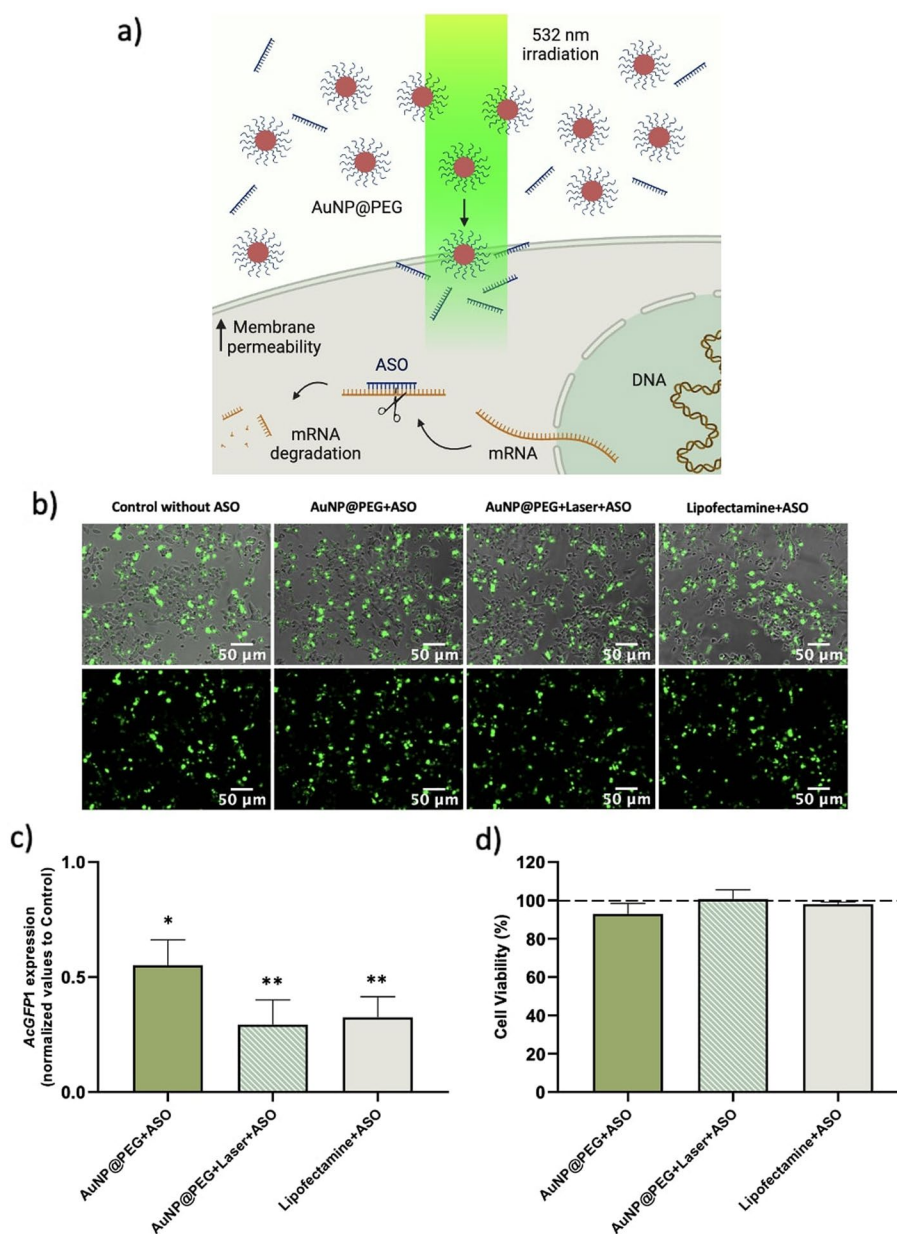


Fig. 4 Overall concept of laser-induced transfection, fluorescence microscopy images of HCT116, RT-qPCR analysis, and cell viability assay. **a** Overall concept of the transfection of the silencing oligonucleotide mediated by mild phototherapy—upon irradiation, AuNPs induce cell uptake and the silencing oligonucleotide (siRNA/ASO) enters the cells (Created with BioRender.com). **b** Fluorescence microscopy images of HCT116 transiently expressing AcGFP1 protein 24 h after silencing experiment in the different conditions tested. Scale bars correspond to 50 μm. **c** *AcGFP1* gene expression in different conditions tested. Gene expression levels were normalised to the cells without *anti-AcGFP1* (Control). Black asterisks indicate statistical differences between samples and Control (* $p < 0.05$; ** $p < 0.01$; Unpaired parametric t test with Welch’s correction). Data represents the mean value \pm the standard error mean of at least three biologically independent experiments with two technical replicates for each. **d** Cell viability analysis of the different experiments with two technical replicates for each. The three conditions tested were normalised to Control. Statistical differences were not observed between all the samples tested with cell control without *anti-AcGFP1* (Control). Data represents the mean value \pm the standard error mean of two biologically independent experiments with two technical replicates for each

than the colorectal model cell line HCT116 (Mokhtary et al. 2018; Yu et al. 2016). In addition, these cells constitutively express GFP and do not require prior use of transfection agents (like lipofectamine) for GFP expression, thus constituting a more challenging model to transfect the siRNA. Cells were incubated with 10 nM of AuNP@PEG for 4 h at 37 °C, then the cells' culture medium was replaced with DMEM without phenol red at (37 °C) containing 20 nM of *anti-copGFP* and irradiated at 2.37 W/cm² for 60 s. Irradiated and non-irradiated cells were allowed to recover for 6 h or 24 h, and *copGFP* expression was analysed by RT-qPCR and fluorescence microscopy at each time point (see Additional file 1: Figure S6).

Mild phototherapy significantly reduced *copGFP* expression by 50% at 6 h and 24 h—see Fig. 5a. This silencing efficacy is comparable to that attained for the commercial Lipofectamine reagent. The quantitative analysis of corrected total cell fluorescence (CTCF) of microscopy images at 6 h and 24 h post-transfection corroborates the silencing of gene expression. A similar reduction of *copGFP* protein expression may be observed at 6 h and 24 h for AuNP@PEG + Laser + ASO and Lipofectamine + ASO—Fig. 5b. Several reports describe the cytotoxicity of cationic lipid reagents (Kasai et al. 2019; Tenchov

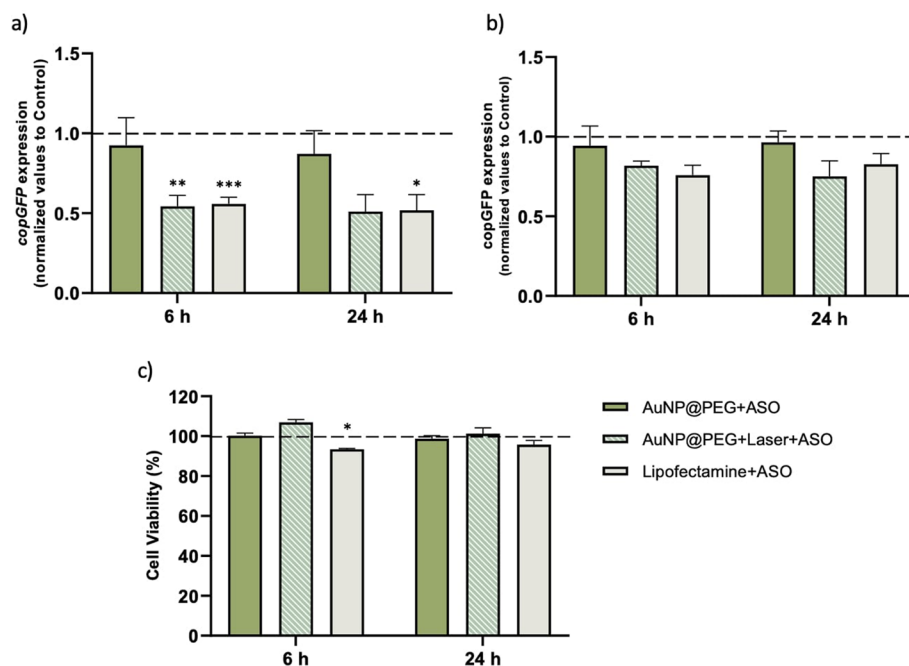


Fig. 5 RT-qPCR analysis, CTCF evaluation of the fluorescence microscopy images of MCF-7/GFP and cell viability assay. **a** *copGFP* gene expression in different conditions tested at 6 h and 24 h. Gene expression levels were normalised to the cells without *anti-copGFP* (Control). Black asterisks denote statistical differences between samples and the Control (* $p < 0.05$; ** $p < 0.01$; *** $p < 0.001$; two-way ANOVA—Mixed-effects analysis with Tukey’s multiple comparison test). Data represents the mean value \pm the standard error mean of at least three biologically independent experiments with two technical replicates for each. **b** CTCF analysis to evaluate *copGFP* protein expression at 6 h and 24 h post-transfection. Statistical differences were not observed between all the samples tested with control without *anti-copGFP* (Control). Data represent the mean value \pm the standard error mean of two biologically independent experiments with three technical replicates each. **c** Cell viability analysis of the different samples tested after 6 h and 24 h of *copGFP* silencing via MTS assay. The three conditions tested were normalised to control. Statistical differences were observed between the cells treated with lipofectamine and cells without *anti-copGFP* (Control). Data represent the mean value \pm the standard error mean of at least three biologically independent experiments with two technical replicates each

et al. 2012). However, our mild phototherapy approach for oligonucleotide transfection does not have an impact on the cells' viability contrary to Lipofectamine—see Fig. 5c.

Mild phototherapy for silencing *c-MYC* proto-oncogene

We then evaluated the efficacy of the mild phototherapy combined with AuNP@*c-MYC* in silencing the frequently overexpressed *c-MYC* oncogene. Indeed, *c-MYC* is a suitable model for gene silencing concepts for eventual gene therapy approaches since this proto-oncogene is a well-known transcription factor involved in cell cycle homeostasis and often dysregulated in cancer cells (Duffy et al. 2021; Strippoli et al. 2020), and several studies have reported its efficacious silencing by ASO vectorised by AuNPs (Conde et al. 2012; Huo et al. 2019; Susnik et al. 2023).

We first optimised the *c-MYC* silencing at different time points (6 h, 9 h, 12 h, and 24 h) in HCT116 2D cells using AuNP@*c-MYC*, using AuNP@PEG 30% and AuNP@*scramble* as controls. An effective decrease of *c-MYC* expression of approximately 70% was observed at 9 h, which was then selected for subsequent experiments (see Additional file 1: Figure S7). Cells were challenged for 9 h with the Au-nanoconjugates and laser irradiation was conducted 4 h post Au-nanoconjugate challenge. Cell viability was assessed by the MTS Assay, *c-MYC* expression was analysed by RT-qPCR, and the *c-MYC* protein expression was evaluated via Immunofluorescence assay (see Additional file 1: Figures S8 and S9).

Figure 6 shows the significant reduction of *c-MYC* expression (25% silencing compared to untreated cells Control, $2^{\Delta\Delta Ct} = 1$). This silencing effect was higher than that obtained for AuNP@*c-MYC* alone (approximately 20%). The quantitative analysis of CTCF of fluorescence microscopy images shows a reduction of *c-MYC* protein expression corroborating the data attained for the mild phototherapy using AuNP@*c-MYC*.

A small decrease in cell viability upon 9 h of silencing compared to untreated cells is observed which might be attributed to the downregulation of *c-MYC* itself, which would have an impact on cell proliferation (Russo et al. 2003; Santo et al. 2023).

Spheroids are 3D cell models that more closely resemble the in vivo behaviour of cell growth than the standard 2D monolayer culture (Abbas et al. 2023; Jubelin et al. 2022; Pinto et al. 2020). As such, we used HCT116 3D spheroids models for a final proof-of-concept for *c-MYC* silencing. Following spheroid's growth for 3 or 7 days, they were challenged with Au-nanoconjugates and *c-MYC* silencing was evaluated as described above for 2D cell cultures (see Additional file 1: Figures S10–S13). The impact on the spheroids' viability was assessed using the LIVE/DEAD Viability/Cytotoxicity assay (see Additional file 1: Figures S14 and S15) and the LDH assay (see Additional file 1: Figure S16).

Figure 7 highlights the effective silencing of the *c-MYC* for the mild phototherapy conditions in 7-day spheroids (AuNP@*c-MYC* + Laser), with a 30% reduction in the expression of *c-MYC*. In addition, statistically significant differences between AuNP@*c-MYC* + Laser and AuNP@*c-MYC* highlight the effect of laser irradiation (phototherapy) to potentiate *c-MYC* silencing. Interestingly, our mild phototherapy did not show the same pronounced reduction of *c-MYC* expression in the 3-day spheroids. This might be because 3-day spheroids are actively proliferating, where *c-MYC* is continuously being

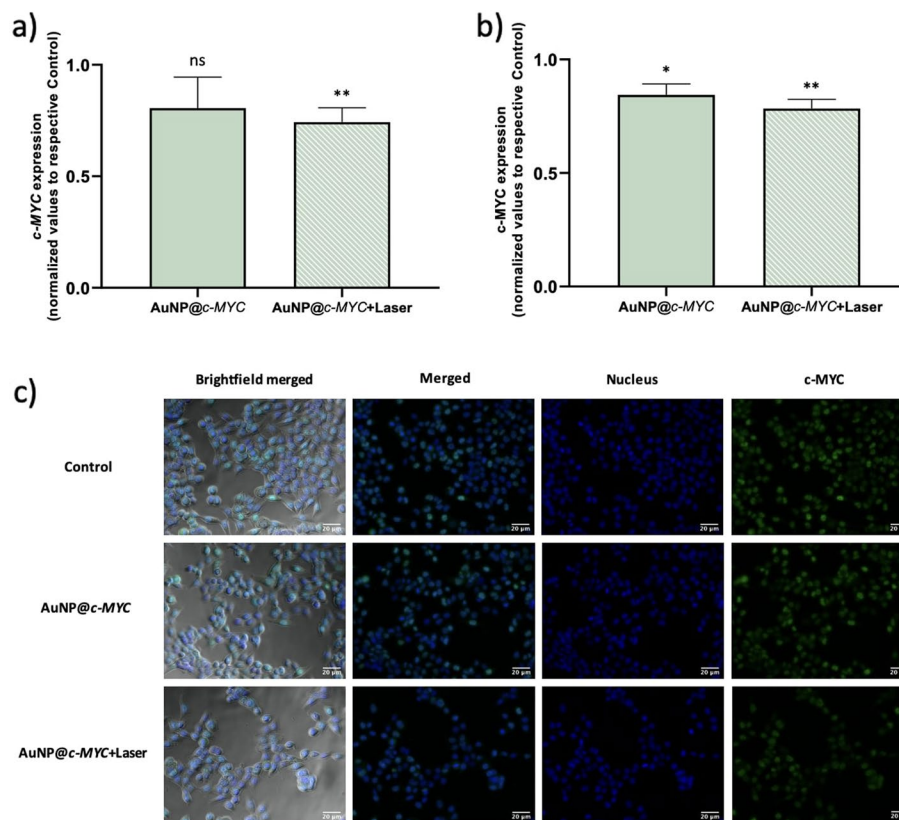


Fig. 6 RT-qPCR analysis and CTCF evaluation of *c-MYC* protein expression by Immunofluorescence assay of HCT116 2D cells. **a** *c-MYC* gene expression at 9 h of gene silencing. Gene expression levels were normalised to respective Controls. Black asterisks indicate statistical differences between samples and Control (** $p < 0.01$; ns—not statistically significant; Unpaired parametric *t* test with Welch’s correction). Data represent the mean value \pm the standard error mean of at least three biologically independent experiments with two technical replicates each. **b** CTCF analysis via Immunofluorescence assay to evaluate *c-MYC* protein expression at 9 h of gene silencing. Black asterisks indicate statistical differences between the samples and Control (* $p < 0.05$; ** $p < 0.01$; Unpaired parametric *t* test with Welch’s correction). Data represents the mean value \pm the standard error mean of two biologically independent experiments with three technical replicates each. **c** Fluorescence microscopy images of 9 h after silencing experiment in Control, AuNP@c-MYC + Laser, and AuNP@c-MYC samples. Scale bars correspond to 20 μm

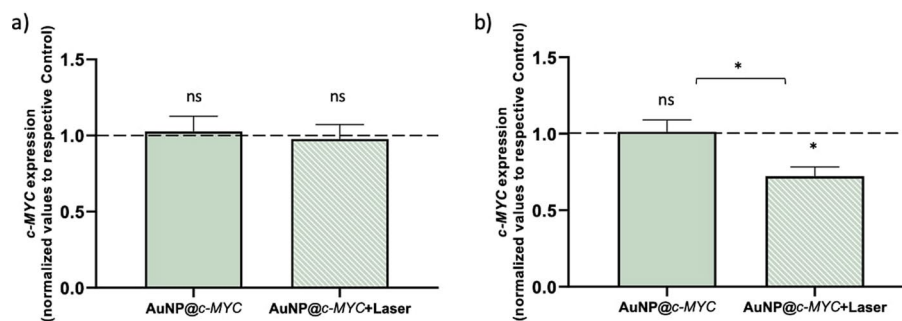


Fig. 7 *c-MYC* gene silencing in 3- and 7-day HCT116 3D spheroids. *c-MYC* gene expression at 9 h of gene silencing in **a** 3-day spheroids and **b** 7-day spheroids. Gene expression levels were normalised to the respective Controls. Black asterisks indicate statistical differences between samples and the Control (* $p < 0.05$; ns not statistically significant; Unpaired parametric *t* test with Welch’s correction). Data represents the mean value \pm the standard error mean of at least three biologically independent experiments with two technical replicates for each

positively induced (Bialkowska et al. 2020; Nayak et al. 2023; Valente et al. 2023). Still, there is a reduction of 5% in AuNP@*c-MYC* + Laser samples in 3-day spheroids (Fig. 7a).

Quantitative analysis of CTCF of fluorescence microscopy denotes a slight decrease of *c-MYC* protein expression between AuNP@*c-MYC* and AuNP@*c-MYC* + Laser in 3-day spheroids (10% and 20%, respectively)—Fig. 8a, c. A 20% reduction in *c-MYC* could be observed for the mild phototherapy in 7-day spheroids—Fig. 8b, d.

The impact of *c-MYC* silencing on cell viability in non-irradiated and irradiated spheroids was assessed by LDH assay and LIVE/DEAD Viability/Cytotoxicity assay (Fig. 9). The ratio between Calcein AM and EthD-1 was calculated since the living cells active intracellular esterase to cleavage the cell-permeant Calcein AM to intensely fluorescent Calcein (Live cells), and EthD-1 is a cell-impermeant that enters in cells with compromised membranes (Dead cells). Irradiated 3-day spheroids show a compromise cell membrane as indicated by the statistically significant decrease to the Calcein AM/EthD-1 ratio, 1.4-fold, and twofold for AuNP@PEG + Laser and AuNP@*c-MYC* + Laser more than Control, respectively—see Fig. 9a. In 7-day spheroids, a slight reduction to the Calcein AM/EthD-1 ratio in AuNP@PEG + Laser and AuNP@*c-MYC* + Laser (around 1.2-fold more) compared to Control is observed although without statistical significance—Fig. 9b. These observations are corroborated by those attained by the LDH assay, where 3-day spheroids showed a threefold and 3.3-fold higher LDH activity for AuNP@PEG + Laser and AuNP@*c-MYC* + Laser compared to Control (see Additional file 1: Figure S16) and in 7-day spheroids were observed approximately 1.7-fold more than Control. These observations are in agreement with previous reports using AuNP or other photothermal agents with laser irradiation (Bromma et al. 2023; Camarero et al. 2023; Pereira et al. 2017).

Few studies have reported the combination of laser irradiation and AuNP for gene silencing in a 3D spheroids model (Huo et al. 2019; Lazzari et al. 2017). Small gold nanoparticles seem to penetrate more than larger AuNPs, indicating that internalisation into spheroids depends on the size of AuNP (Huang et al. 2012; Oliveira et al. 2024). Huang *et al.* developed a pulsed NIR light-based technique for the spatiotemporal control of gene silencing in 3D-cultured human embryonic stem cells, using siRNA covalently attached to hollow gold nanoshells (Xiao Huang et al. 2016). In addition, 3-day spheroids were more sensitive to localised heat compared to 7-day spheroids, which reinforces the need for the characterisation of spheroid size and structure, cells–cells contact, and TME modifications to allow comparison between gene silencing studies with AuNP@ASO combined with photo-irradiation.

Conclusions

Herein, we demonstrate for the first time the effective silencing of *c-MYC* via mild phototherapy in colorectal carcinoma 3D spheroids. The use of low concentrations of Au-nanoconjugates combined with an LDI 2.37 W/cm² for 60 s shows no impact on cell viability but allows for improved uptake into the cell. The mild phototherapy might trigger modification of the fluidity and permeability of the cell membrane, potentiating uptake. Our mild phototherapy approach was able to attain comparable silencing to that of a commercial Lipofectamine reagent but with less cytotoxic effect on the MCF-7/GFP cells. Moreover, our results highlight the enhancement of *c-MYC* silencing in HCT116

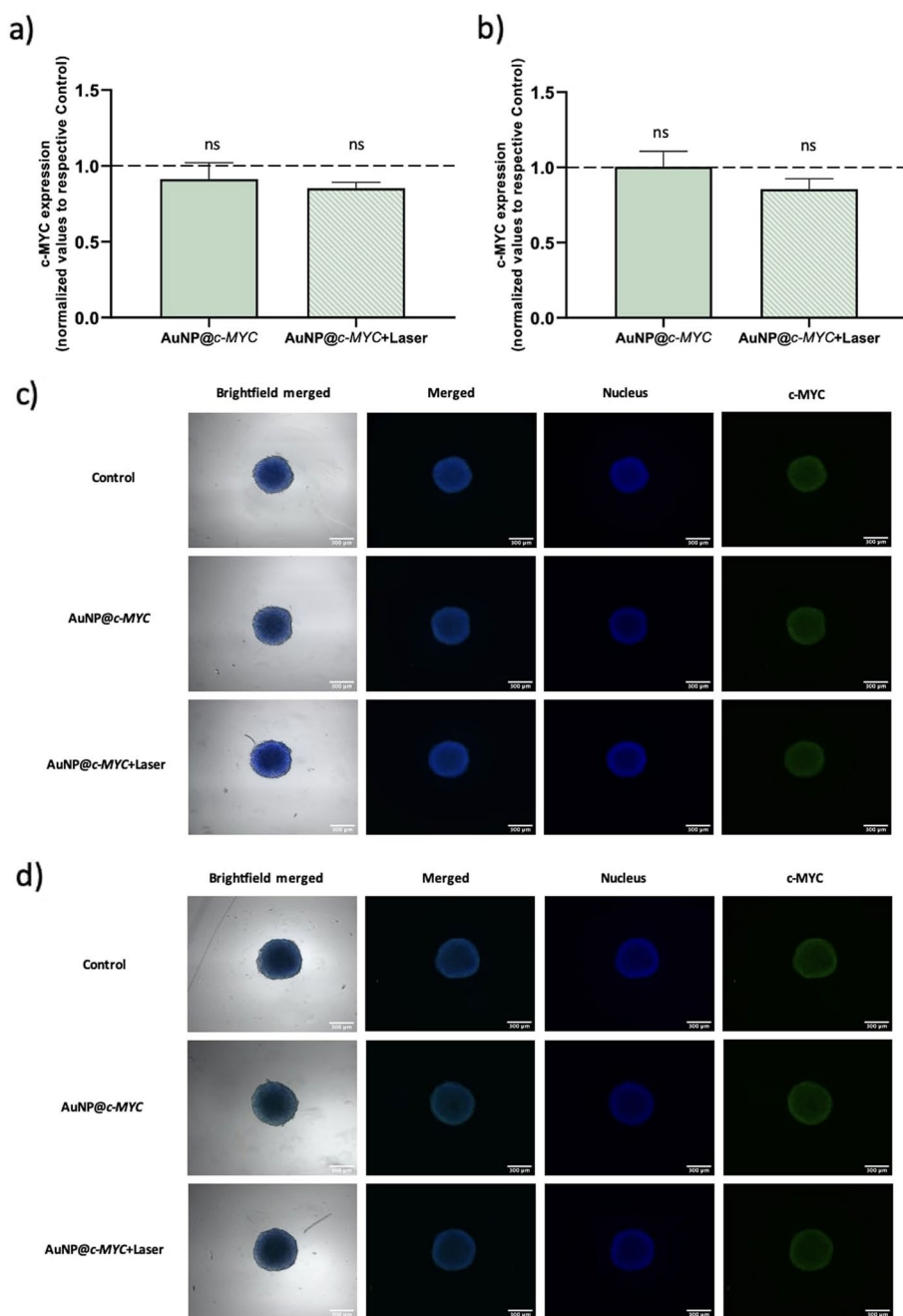


Fig. 8 CTCF evaluation of c-MYC protein expression in 3- and 7-day HCT116 spheroids. CTCF analysis of Immunofluorescence assay evaluates c-MYC protein expression at 9 h after gene silencing in **(a)** 3-day spheroids and **(b)** 7-day spheroids. Statistical differences were not observed between the samples tested with Control (ns not statistically significant; Unpaired parametric *t* test with Welch's correction). Data represent the mean value \pm the standard error mean of two biologically independent experiments with three technical replicates for each. **c** Fluorescence microscopy images of Control, AuNP@c-MYC, and AuNP@c-MYC + Laser sample in 3-day spheroids. Scale bars correspond to 300 μm. **d** Same as for c) in 7-day spheroid

2D cells and 7-day 3D spheroids due to the proposed mild phototherapy to improve the internalisation of AuNP@c-MYC. The complexity of 3D cell growth showed that there is a clear difference in sensitivity of 3-day spheroids to localised heat compared to 7-day

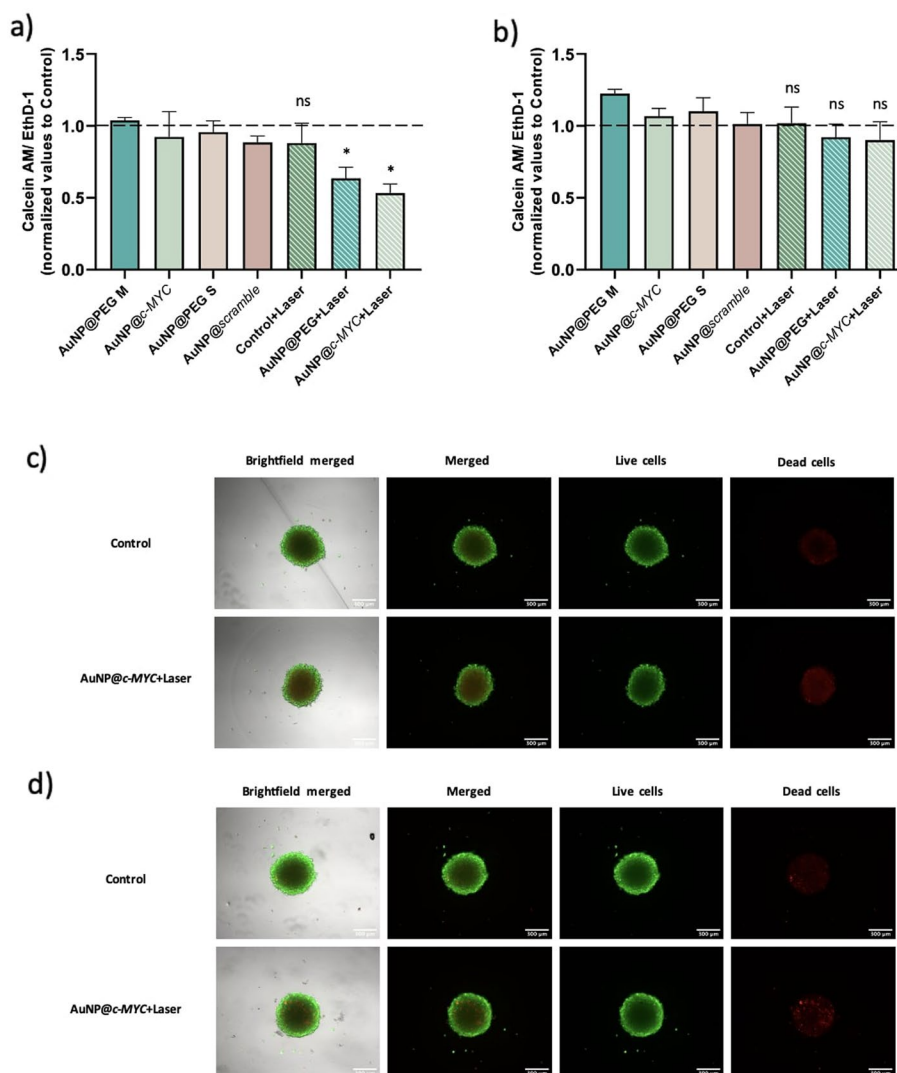


Fig. 9 Cell viability/cytotoxicity in 3- and 7-day HCT116 3D spheroids. Cell viability/cytotoxicity evaluation of the different samples tested after 9 h of *c-MYC* silencing via LIVE/DEAD Viability/Cytotoxicity assay in **(a)** 3-day spheroids and **(b)** 7-day spheroids. The seven conditions tested were normalised to untreated cells (Control). Statistical differences were observed between AuNP@PEG + Laser and AuNP@c-MYC + Laser with control in 3-day spheroids. Black asterisks indicate statistical differences between samples and the Control (* $p < 0.05$; ns not statistically significant; Unpaired parametric t test with Welch's correction). Data represents the mean value \pm the standard error mean of two biologically independent experiments with three technical replicates each. **c** Calcein AM/EthD-1 fluorescence microscopy images of control and AuNP@c-MYC + Laser in 3-day spheroids. Scale bars correspond to 300 μm . **d** Same as c) in 7-day spheroid

spheroids, which reinforces the relevance of correlating data of gene silencing and cell viability considering the volume of the spheroids and respective cell number/density.

Supplementary Information

The online version contains supplementary material available at <https://doi.org/10.1186/s12645-024-00256-4>.

Additional file 1: Table S1. Physicochemical characteristics AuNP and Au-nanoconjugates measured by DLS, ζ -potential and their polydispersity index. **Table S2.** Primer sequences used in RT-qPCR. *FW* Forward primer. *RV* Reverse primer. **Table S3.** Antisense oligonucleotides and antisense sequences used for gene silencing. **Figure S1.** Hydrodynamic size distribution of Au-nanoconjugates measured via DLS in water as described in Material and

Methods. **Figure S2.** UV–Vis spectra of Au-nanoconjugates, and TEM images to evaluate the diameter size of the AuNP core. **Figure S3.** Trypan blue exclusion assay of HCT116 2D cells. **Figure S4.** Cell viability and cytotoxic assay of HCT116 2D cells. **Figure S5.** pAcGFP1–Nuc Vector. **Figure S6.** Fluorescence microscopy images of MCF-7 2D cells constitutively expressing *copGFP* gene. **Figure S7.** Evaluation of *c-MYC* expression using RT-qPCR at different time points in HCT116 2D cells. **Figure S8.** RT-qPCR analysis of *c-MYC* silencing and cell viability assay in HCT116 2D cells. **Figure S9.** CTCF evaluation of *c-MYC* protein expression by fluorescence microscopy images of HCT116 2D cells. **Figure S10.** RT-qPCR analysis of *c-MYC* silencing and CTCF evaluation of *c-MYC* protein expression in 3-day spheroids. **Figure S11.** RT-qPCR analysis of *c-MYC* silencing and CTCF evaluation of *c-MYC* protein expression in 7-day spheroids. **Figure S12.** Fluorescence microscopy images in 3-day spheroids by Immunofluorescence assay. **Figure S13.** Fluorescence microscopy images in 7-day spheroids by Immunofluorescence assay. **Figure S14.** Fluorescence microscopy images in 3-day spheroids by Live/DEAD Viability/ Cytotoxicity assay. **Figure S15.** Fluorescence microscopy images in 7-day spheroids by Live/DEAD Viability/ Cytotoxicity assay. **Figure S16.** LDH activity analysis after 9 h of *c-MYC* silencing via LDH Assay in 3D spheroids.

Acknowledgements

Not applicable.

Author contributions

DF: formal analysis, investigation, methodology, validation, writing—original draft, writing—review and editing. ARF: conceptualisation, funding acquisition, project administration, supervision, validation, writing—review and editing. PVB: conceptualisation, funding acquisition, project administration, supervision, validation, writing—review and editing.

Funding

This work is financed by national funds from FCT—Fundação para a Ciência e a Tecnologia, I.P., in the scope of the project UIDP/04378/2020 (<https://doi.org/10.54499/UIDP/04378/2020>) and UIDB/04378/2020 (<https://doi.org/10.54499/UIDB/04378/2020>) of the Research Unit on Applied Molecular Biosciences—UCIBIO and the project LA/P/0140/2020 of the Associate Laboratory Institute for Health and Bioeconomy—i4HB and in the scope of the project NANOHEAT – <https://doi.org/https://doi.org/10.54499/2022.04315.PTDC>. PVB acknowledges 2021.09768.CBM. DF also acknowledges FCT.IP for the PhD Grant (2020.06599.BD).

Availability of data and materials

All data generated or analysed during this study are included in this published article [and its Additional files].

Declarations

Ethics approval and consent to participate

Not applicable.

Consent for publication

All authors agree to publish.

Competing interests

The authors declare that they have no competing interests.

Received: 14 February 2024 Accepted: 16 March 2024

Published online: 22 March 2024

References

- Abbas ZN, Al-Saffar AZ, Jasim SM, Sulaiman GM (2023) Comparative analysis between 2D and 3D colorectal cancer culture models for insights into cellular morphological and transcriptomic variations. *Sci Rep* 13(1):1–16. <https://doi.org/10.1038/s41598-023-45144-w>
- Amendoeira A, García LR, Fernandes AR, Baptista PV (2020) Light irradiation of gold nanoparticles toward advanced cancer therapeutics. *Adv Ther* 3(1):1900153. <https://doi.org/10.1002/adtp.201900153>
- Baptista P, Conde J, Rosa J, Baptista P (2013) Gold-Nanobeacons as a theranostic system for the detection and inhibition of specific genes. *Protoc Exch*. <https://doi.org/10.1038/protex.2013.088>
- Beola L, Asín L, Roma-Rodrigues C, Fernandez-Afonso Y, Fratila RM, Serantes D, Ruta S, Chantrell RW, Fernandes AR, Baptista PV, de la Fuente JM, Grazu V, Gutierrez L (2020) The intracellular number of magnetic nanoparticles modulates the apoptotic death pathway after magnetic hyperthermia treatment. *ACS Appl Mater Interfaces* 12(39):43474–43487. <https://doi.org/10.1021/acsami.0c12900>
- Białkowska K, Komorowski P, Bryszewska M, Miłowska K (2020) Spheroids as a type of three-dimensional cell cultures—examples of methods of preparation and the most important application. *Int J Mol Sci* 21(17):1–17. <https://doi.org/10.3390/IJMS21176225>
- Braun GB, Pallaro A, Wu G, Missirlis D, Zasadzinski JA, Tirrell M, Reich NO (2009) Laser-activated gene silencing via gold nanoshell-siRNA conjugates. *ACS Nano* 3(7):2007–2015. <https://doi.org/10.1021/nn900469q>

- Bromma K, Beckham W, Chithrani DB (2023) Utilizing two-dimensional monolayer and three-dimensional spheroids to enhance radiotherapeutic potential by combining gold nanoparticles and docetaxel. *Cancer Nanotechnol* 14(1):1–26. <https://doi.org/10.1186/s12645-023-00231-5>
- Camarero P, Haro-González P, Quintanilla M (2023) Near infrared laser irradiation on single multicellular spheroids. *Opt Mater* 142:114055. <https://doi.org/10.1016/j.optmat.2023.114055>
- Carballo-Pedraes N, Ponti F, Lopez-Seijas J, Miranda-Balbuena D, Bono N, Candiani G, Rey-Rico A (2023) Non-viral gene delivery to human mesenchymal stem cells: a practical guide towards cell engineering. *J Biol Eng* 17(1):1–24. <https://doi.org/10.1186/S13036-023-00363-7>
- Carnovale C, Bryant G, Shukla R, Bansal V (2019) Identifying trends in gold nanoparticle toxicity and uptake: size, shape, capping ligand, and biological corona. *ACS Omega* 4(1):242–256. <https://doi.org/10.1021/acsomega.8b03227>
- Conde J, Ambrosone A, Sanz V, Hernandez Y, Marchesano V, Tian F, Child H, Berry CC, Ibarra MR, Baptista PV, Tortiglione C, De La Fuente JM (2012) Design of multifunctional gold nanoparticles for in vitro and in vivo gene silencing. *ACS Nano* 6(9):8316–8324. <https://doi.org/10.1021/nn3030223>
- Cory AH, Owen TC, Bartrop JA, Cory JG (1991) Use of an aqueous soluble tetrazolium/formazan assay for cell growth assays in culture. *Cancer Commun* 3(7):207–212. <https://doi.org/10.3727/095535491820873191>
- Decker T, Lohmann-Matthes ML (1988) A quick and simple method for the quantitation of lactate dehydrogenase release in measurements of cellular cytotoxicity and tumor necrosis factor (TNF) activity. *J Immunol Methods* 115(1):61–69. [https://doi.org/10.1016/0022-1759\(88\)90310-9](https://doi.org/10.1016/0022-1759(88)90310-9)
- Deng HY, Wang L, Tang D, Zhang Y, Zhang L (2021) Review on the laser-induced performance of photothermal materials for ignition application. *Energ Mater Front* 2(3):201–217. <https://doi.org/10.1016/J.ENMF.2021.08.001>
- Duffy MJ, O'Grady S, Tang M, Crown J (2021) MYC as a target for cancer treatment. *Cancer Treat Rev*. <https://doi.org/10.1016/j.ctrv.2021.102154>
- Elsner M (2012) Single-stranded siRNAs for in vivo gene silencing. *Nat Biotechnol* 30(11):1063–1063. <https://doi.org/10.1038/nbt.2413>
- Ferreira D, Fontinha D, Martins C, Pires D, Fernandes AR, Baptista PV (2020) Gold nanoparticles for vectorization of nucleic acids for cancer therapeutics. *Molecules* 25(15):3489. <https://doi.org/10.3390/MOLECULES25153489>
- Fus-Kujawa A, Prus P, Bajdak-Rusinek K, Teper P, Gawron K, Kowalczyk A, Sieron AL (2021) An overview of methods and tools for transfection of eukaryotic cells in vitro. *Front Bioeng Biotechnol*. <https://doi.org/10.3389/fbioe.2021.701031>
- Graczyk A, Pawłowska R, Chworos A (2021) Gold nanoparticles as carriers for functional RNA nanostructures. *Bioconjug Chem* 32(8):1667–1674. <https://doi.org/10.1021/acs.bioconjchem.1c00211>
- Han HS, Choi KY (2021) Advances in nanomaterial-mediated photothermal cancer therapies: toward clinical applications. *Biomedicines*. <https://doi.org/10.3390/biomedicines9030305>
- Heinemann D, Schomaker M, Kalies S, Schieck M, Carlson R, Escobar HM, Ripken T, Meyer H, Heisterkamp A (2013) Gold nanoparticle mediated laser transfection for efficient siRNA mediated gene knock down. *PLoS ONE*. <https://doi.org/10.1371/journal.pone.0058604>
- Hosseini SA, Kardani A, Yaghoobi H (2023) A comprehensive review of cancer therapies mediated by conjugated gold nanoparticles with nucleic acid. *Int J Biol Macromol*. <https://doi.org/10.1016/j.ijbiomac.2023.127184>
- Hu X, Zhang Y, Ding T, Liu J, Zhao H (2020) Multifunctional gold nanoparticles: a novel nanomaterial for various medical applications and biological activities. *Front Bioeng Biotechnol* 8:556510. <https://doi.org/10.3389/fbioe.2020.00990>
- Huang X, El-Sayed MA (2010) Gold nanoparticles: optical properties and implementations in cancer diagnosis and photothermal therapy. *J Adv Res* 1(1):13–28. <https://doi.org/10.1016/J.JARE.2010.02.002>
- Huang K, Ma H, Liu J, Huo S, Kumar A, Wei T, Zhang X, Jin S, Gan Y, Wang PC, He S, Zhang X, Liang XJ (2012) Size-dependent localization and penetration of ultrasmall gold nanoparticles in cancer cells, multicellular spheroids, and tumors in vivo. *ACS Nano* 6(5):4483–4493. <https://doi.org/10.1021/nn301282m>
- Huang X, Hu Q, Lai Y, Morales DP, Clegg DO, Reich NO (2016) Light-patterned RNA interference of 3D-cultured human embryonic stem cells. *Adv Mater* 28(48):10732–10737. <https://doi.org/10.1002/adma.201603318>
- Huo S, Gong N, Jiang Y, Chen F, Guo H, Gan Y, Wang Z, Herrmann A, Liang XJ (2019) Gold-DNA nanosunflowers for efficient gene silencing with controllable transformation. *Sci Adv*. <https://doi.org/10.1126/sciadv.aaw6264>
- Janic B, Liu F, Bobbitt KR, Brown SL, Chetty IJ, Mao G, Movsas B, Wen N (2018) Cellular uptake and radio-sensitization effect of small gold nanoparticles in MCF-7 breast cancer cells. *J Nanomed Nanotechnol*. <https://doi.org/10.4172/2157-7439.1000499>
- Jensen C, Teng Y (2020) Is it time to start transitioning from 2D to 3D cell culture? *Front Mol Biosci* 7:513823. <https://doi.org/10.3389/FMOLB.2020.00033/BIBTEX>
- Jubelin C, Muñoz-García J, Griscom L, Cochonneau D, Ollivier E, Heymann MF, Vallette FM, Oliver L, Heymann D (2022) Three-dimensional in vitro culture models in oncology research. *Cell Biosci*. <https://doi.org/10.1186/s13578-022-00887-3>
- Kang P, Li X, Liu Y, Shiers SI, Xiong H, Giannotta M, Dejana E, Price TJ, Randrianalisoa J, Nielsen SO, Qin Z (2019) Transient photoinactivation of cell membrane protein activity without genetic modification by molecular hyperthermia. *ACS Nano* 13(11):12487–12499. <https://doi.org/10.1021/acsnano.9b01993>
- Kanu GA, Parambath JBM, Abu Odeh RO, Mohamed AA (2022) Gold nanoparticle-mediated gene therapy. *Cancers*. <https://doi.org/10.3390/cancers14215366>
- Kasai H, Inoue K, Imamura K, Yuvienco C, Montclare JK, Yamano S (2019) Efficient siRNA delivery and gene silencing using a lipopolyptide hybrid vector mediated by a caveolae-mediated and temperature-dependent endocytic pathway. *J Nanobiotechnol* 17(1):1–14. <https://doi.org/10.1186/s12951-019-0444-8>
- Khorkova O, Stahl J, Joji A, Volmar CH, Wahlestedt C (2023) Amplifying gene expression with RNA-targeted therapeutics. *Nat Rev Drug Discov* 22(7):539–561. <https://doi.org/10.1038/s41573-023-00704-7>
- Kim D, Paik J, Kim H (2023) Effect of gold nanoparticles distribution radius on photothermal therapy efficacy. *Sci Rep* 13(1):1–13. <https://doi.org/10.1038/s41598-023-39040-6>
- Krajczewski J, Kołataj K, Kudelski A (2017) Plasmonic nanoparticles in chemical analysis. *RSC Adv* 7(28):17559–17576. <https://doi.org/10.1039/c7ra01034f>

- Kumar PPP, Lim D-K, Prabhakaran P, Kumar P, Lim D-K (2023) Photothermal Effect of gold nanoparticles as a nanomedicine for diagnosis and therapeutics. *Pharmaceutics* 15(9):2349. <https://doi.org/10.3390/PHARMACEUTICS15092349>
- Lazzari G, Couvreur P, Mura S (2017) Multicellular tumor spheroids: a relevant 3D model for the: in vitro preclinical investigation of polymer nanomedicines. *Polym Chem* 8(34):4947–4969. <https://doi.org/10.1039/c7py00559h>
- Lee PC, Meisel D (1982) Adsorption and surface-enhanced Raman of dyes on silver and gold sols. *J Phys Chem* 86(17):3391–3395. <https://doi.org/10.1021/j100214a025>
- Lenis-Rojas OA, Roma-Rodrigues C, Fernandes AR, Marques F, Pérez-Fernández D, Guerra-Varela J, Sánchez L, Vázquez-García D, López-Torres M, Fernández A, Fernández JJ (2017) Dinuclear Ru(II)(bipy)2 derivatives: structural, biological, and in vivo zebrafish toxicity evaluation. *Inorg Chem* 56(12):7127–7144. <https://doi.org/10.1021/acs.inorgchem.7b00790>
- Livak KJ, Schmittgen TD (2001) Analysis of relative gene expression data using real-time quantitative PCR and the 2- $\Delta\Delta$ CT method. *Methods* 25(4):402–408. <https://doi.org/10.1006/meth.2001.1262>
- Madrid M (2018) Plasmonic intracellular delivery. *Plasmonics*. <https://doi.org/10.5772/intechopen.79384>
- Mendes R, Pedrosa P, Lima JC, Fernandes AR, Baptista PV (2017) Photothermal enhancement of chemotherapy in breast cancer by visible irradiation of Gold Nanoparticles. *Sci Rep* 7(1):1–9. <https://doi.org/10.1038/s41598-017-11491-8>
- Mokhtary P, Javan B, Sharbatkhari M, Soltani A, Erfani-Moghadam V (2018) Cationic vesicles for efficient shRNA transfection in the MCF-7 breast cancer cell line. *Int J Nanomed* 13:7107–7121. <https://doi.org/10.2147/IJN.S177674>
- Mollé LM, Smyth CH, Yuen D, Johnston APR (2022) Nanoparticles for vaccine and gene therapy: overcoming the barriers to nucleic acid delivery. *Wiley Interdiscip Rev Nanomed Nanobiotechnol* 14(6):1809. <https://doi.org/10.1002/WNAN.1809>
- Nayak P, Bentivoglio V, Varani M, Signore A (2023) Three-dimensional in vitro tumor spheroid models for evaluation of anticancer therapy: recent updates. *Cancers* 15(19):4846. <https://doi.org/10.3390/CANCERS15194846>
- Oliveira BB, Ferreira D, Fernandes AR, Baptista PV (2023) Engineering gold nanoparticles for molecular diagnostics and biosensing. *Wiley Interdiscip Rev Nanomed Nanobiotechnol* 15(1):e1836. <https://doi.org/10.1002/wnan.1836>
- Oliveira BB, Fernandes AR, Baptista PV (2024) Assessing the gene silencing potential of AuNP-based approaches on conventional 2D cell culture versus 3D tumor spheroid. *Front Bioeng Biotechnol* 12:1320729. <https://doi.org/10.3389/fbioe.2024.1320729>
- Overchuk M, Weersink RA, Wilson BC, Zheng G (2023) Photodynamic and photothermal therapies: synergy opportunities for nanomedicine. *ACS Nano* 17(9):7979–8003. <https://doi.org/10.1021/acsnano.3c00891>
- Pedrosa P, Heuer-Jungemann A, Kanaras AG, Fernandes AR, Baptista PV (2017) Potentiating angiogenesis arrest in vivo via laser irradiation of peptide functionalised gold nanoparticles. *J Nanobiotechnol* 15(1):1–8. <https://doi.org/10.1186/s12951-017-0321-2>
- Pedrosa P, Mendes R, Cabral R, Martins LMDRS, Baptista PV, Fernandes AR (2018) Combination of chemotherapy and Au-nanoparticle phototherapy in the visible light to tackle doxorubicin resistance in cancer cells. *Sci Rep* 8(1):1–8. <https://doi.org/10.1038/s41598-018-29870-0>
- Pereira PMR, Berisha N, Bhupathiraju NVSDK, Fernandes R, Tomé JPC, Drain CM (2017) Cancer cell spheroids are a better screen for the photodynamic efficiency of glycosylated photosensitizers. *PLoS ONE*. <https://doi.org/10.1371/journal.pone.0177737>
- Pinto B, Henriques AC, Silva PMA, Bousbaa H (2020) Three-dimensional spheroids as in vitro preclinical models for cancer research. *Pharmaceutics* 12(12):1–38. <https://doi.org/10.3390/pharmaceutics12121186>
- Riley RS, Day ES (2017) Gold nanoparticle-mediated photothermal therapy: applications and opportunities for multimodal cancer treatment. *Wiley Interdiscip Rev Nanomed Nanobiotechnol*. <https://doi.org/10.1002/wnan.1449>
- Roma-Rodrigues C, Pombo I, Fernandes AR, Baptista PV (2020) Hyperthermia induced by gold nanoparticles and visible light phototherapy combined with chemotherapy to tackle doxorubicin sensitive and resistant colorectal tumor 3D spheroids. *Int J Mol Sci* 21(21):1–13. <https://doi.org/10.3390/ijms21218017>
- Russo P, Arzani D, Trombino S, Falugi C (2003) c-myc down-regulation induces apoptosis in human cancer cell lines exposed to RPR-115135 (C31H29NO4), a non-peptidomimetic farnesyltransferase inhibitor. *J Pharmacol Exp Ther* 304(1):37–47. <https://doi.org/10.1124/jpet.102.042952>
- Santo D, Mendonça PV, Serra AC, Coelho JFJ, Faneca H (2023) Targeted downregulation of MYC mediated by a highly efficient lactobionic acid-based glycoconjugate to enhance chemosensitivity in human hepatocellular carcinoma cells. *Int J Pharm* 637:122865. <https://doi.org/10.1016/j.ijpharm.2023.122865>
- Sharma AR, Lee YH, Bat-Ulzii A, Bhattacharya M, Chakraborty C, Lee SS (2022) Recent advances of metal-based nanoparticles in nucleic acid delivery for therapeutic applications. *J Nanobiotechnol* 20(1):1–21. <https://doi.org/10.1186/s12951-022-01650-z>
- Silva TFS, Smoleński P, Martins LMDRS, Guedes Da Silva MFC, Fernandes AR, Luis D, Silva A, Santos S, Borralho PM, Rodrigues CMP, Pombeiro AJL (2013) Cobalt and zinc compounds bearing 1,10-phenanthroline-5,6-dione or 1,3,5-triazza-7-phosphaadamantane derivatives—synthesis, characterization, cytotoxicity, and cell selectivity studies. *Eur J Inorg Chem* 2013(21):3651–3658. <https://doi.org/10.1002/ejic.201300197>
- Stewart MP, Langer R, Jensen KF (2018) Intracellular delivery by membrane disruption: mechanisms, strategies, and concepts. *Chem Rev* 118(16):7409–7531. <https://doi.org/10.1021/acs.chemrev.7b00678>
- Stoddart MJ (2011) Cell Viability Assays: Introduction. In: Stoddart MJ (ed) *Methods in Molecular Biology*, vol 740. Humana Press Inc, Totowa, pp 1–6. https://doi.org/10.1007/978-1-61779-108-6_1
- Strippoli A, Cocomazzi A, Basso M, Cenci T, Ricci R, Pierconti F, Cassano A, Fiorentino V, Barone C, Bria E, Ricci-Vitiani L, Tortora G, Larocca LM, Martini M (2020) C-myc expression is a possible keystone in the colorectal cancer resistance to egfr inhibitors. *Cancers*. <https://doi.org/10.3390/cancers12030638>
- Strober W (2015) Trypan blue exclusion test of cell viability. *Curr Protoc Immunol* 111(1):A3.B1–A3.B3. <https://doi.org/10.1002/0471142735.ima03bs111>
- Susnik E, Bazzoni A, Taladriz-Blanco P, Balog S, Moreno-Echeverri AM, Glaubitz C, Brito Oliveira B, Ferreira D, Viana Baptista P, Petri-Fink A, Rothen-Rutishauser B (2023) Epidermal growth factor alters silica nanoparticle uptake and improves

- gold-nanoparticle-mediated gene silencing in A549 cells. *Front Nanotechnol* 5:1220514. <https://doi.org/10.3389/fnano.2023.1220514>
- Tenchov B, Sugimoto Y, Koynova R, Brueggemeier RW, Lee RJ (2012) Highly efficient cationic ethylphosphatidylcholine siRNA carrier for GFP suppression in modified breast cancer cells. *Anticancer Res* 32(7):2563–2566
- Valente R, Cordeiro S, Luz A, Melo MC, Rodrigues CR, Baptista PV, Fernandes AR (2023) Doxorubicin-sensitive and -resistant colorectal cancer spheroid models: assessing tumor microenvironment features for therapeutic modulation. *Front Cell Dev Biol*. <https://doi.org/10.3389/fcell.2023.1310397>
- Wang P, Chen B, Zhan Y, Wang L, Luo J, Xu J, Zhan L, Li Z, Liu Y, Wei J (2022) Enhancing the efficiency of mild-temperature photothermal therapy for cancer assisting with various strategies. *Pharmaceutics* 14(11):2279. <https://doi.org/10.3390/PHARMACEUTICS14112279>
- Wang C, Pan C, Yong H, Wang F, Bo T, Zhao Y, Ma B, He W, Li M (2023) Emerging non-viral vectors for gene delivery. *J Nanobiotechnol*. <https://doi.org/10.1186/S12951-023-02044-5>
- Yu X, Liang X, Xie H, Kumar S, Ravinder N, Potter J, de du Mollerat J, Chesnut JD (2016) Improved delivery of Cas9 protein/gRNA complexes using lipofectamine CRISPRMAX. *Biotechnol Lett* 38(6):919–929. <https://doi.org/10.1007/s10529-016-2064-9>
- Zanoni M, Cortesi M, Zamagni A, Arienti C, Pignatta S, Tesi A (2020) Modeling neoplastic disease with spheroids and organoids. *J Hematol Oncol* 13(1):1–15. <https://doi.org/10.1186/S13045-020-00931-0/FIGURES/5>
- Zhang J, Chen B, Gan C, Sun H, Zhang J, Feng L (2023) A comprehensive review of small interfering RNAs (siRNAs): mechanism, therapeutic targets, and delivery strategies for cancer therapy. *Int J Nanomed* 18:7605–7635. <https://doi.org/10.2147/IJN.S436038>
- Zhu Y, Zhu L, Wang X, Jin H (2022) RNA-based therapeutics an overview and prospectus. *Cell Death Dis* 13(7):1–15. <https://doi.org/10.1038/s41419-022-05075-2>

Publisher's Note

Springer Nature remains neutral with regard to jurisdictional claims in published maps and institutional affiliations.